JOURNAL OF AIRCRAFT
Vol. 44, No. 3, May–June 2007

Multi-Objective Aerodynamic Exploration of Elements' Setting for High-Lift Airfoil Using Kriging Model

Masahiro Kanazaki*
Japan Aerospace Exploration Agency (JAXA), Tokyo 182-8522, Japan
Kentaro Tanaka†
Ryoyu Systems Company, Ltd., Tokyo 108-0074, Japan
Shinkyu Jeong‡
Tohoku University, Sendai 980-8577, Japan
and
Kazuomi Yamamoto§
Japan Aerospace Exploration Agency (JAXA), Tokyo 182-8522, Japan

DOI: 10.2514/1.25422

A multi-objective design exploration for a three-element airfoil consisting of a slat, a main wing, and a flap was carried out. The lift curve improvement is important to design high-lift system, thus design has to be performed with considered multi-angle. The objective functions considered here are to maximize the lift coefficient at landing and near-stall conditions simultaneously. Genetic algorithm is used as an optimizer. Although it has the advantage of global exploration, its computational cost is expensive. To reduce the computational cost, the Kriging surrogate model, which was constructed based on several sample designs, is introduced. The solution space was explored based on the maximization of expected improvement (EI) value corresponding to objective functions on the Kriging surrogate models. The improvement of Kriging surrogate model and the exploration of the optimum can be advanced at the same time by maximizing EI value. In this study, a total of 90 sample points are evaluated using the Reynolds-averaged Navier–Stokes simulation for the construction of the Kriging surrogate model. Through the present exploration process, several designs were obtained with better performance than the baseline setting in each objective function. To obtain the information of the design space, functional analysis of variance, which is one of the data mining techniques showing the effect of each design variable on the objectives, is applied. Main effects of the design variables are calculated to recognize which design variable has the effect on the objective functions. This result suggests that the gap and the deflection of the flap have a remarkable effect on each objective function and the gap of the slat has an effect at near-stall condition.

Nomenclature

C_l	=	lift coefficient
$C_{l\alpha}$	=	lift coefficient at the angle of attack of α degree
C_p	=	pressure coefficient
c	=	chord length of airfoil when flap and slat are retracted into the main element
$E[I(\cdot)]$	=	expected improvement
$\mathrm{EI}_{C l\alpha}$	=	EI value for $C_{l\alpha}$
$f_{\max}$	=	maximum value among sample points
s^2	=	mean squared error of the predictor
$\hat{y}$	=	predicted value on Kriging surrogate model
$y(\cdot)$	=	unknown function
x	=	scalar component of $\boldsymbol{x}$
$\boldsymbol{x}$	=	vector denoting position in the design space
α	=	angle of attack
$\varepsilon(\cdot)$	=	deviation from constant model
μ	=	constant global model of Kriging surrogate model
Φ	=	standard normal distribution
ϕ	=	standard normal density

Presented as Paper 1471 at the 44th AIAA Aerospace Sciences Meeting and Exhibit, Reno, NV, 9–12 January 2006; received 25 May 2006; revision received 24 August 2006; accepted for publication 29 August 2006.

*Researcher, Civil Transport Team, Aviation Program Group, Chofu. Member AIAA.
†Engineer, Engineering Solution Division, Minato-ku.
‡Research Associate, Institute of Fluid Science. Associate Member AIAA.
§Senior Researcher, Civil Transport Team, Aviation Program Group, Chofu. Member AIAA.

Introduction

A CIVIL aircraft wing is generally designed by considering a cruise condition. On the contrary, when an aircraft lands or takes off, its wing should gain enough lift even at low speed. In such condition, a high-lift system that can increase the wing load at low speed is required. Thus, a high-lift system is one of the main interests in aircraft design due to its effect on landing/takeoff performances and payload capacity of an aircraft.

One of a typical high-lift system is a multi-element wing. The flowfield around a multi-element wing has a complex physics caused by the interaction of each element [1,2]. One of the important physics is *circulation effect*. The circulation of a forward element reduces the leading-edge suction peak of a trailing element, thus delaying separation. Moreover, the trailing element induces a circulation effect on the forward element and increases the loading. Additionally, viscous effect of wakes from each element exists. It provides a damping effect on the pressure peak of trailing element. However, wakes often merge with the boundary layer of the trailing element and boundary layer becomes much thinner; as a result, the separation increases. Thus, the high-lift system should be designed with considering complex flow physics as described. To evaluate such physics, the high-fidelity evaluation of a high-lift system is desirable in a design process.

Recently, many studies have been carried out to develop the high-fidelity flow solver using Navier–Stokes simulation around a high-lift system and they are validated [3–5]. Thus, the relevant design considering accurate flow physics can be expected. To introduce high-fidelity evaluation, it is required to employ high-efficient design

Fig. 1 Baseline airfoil and elements' settings.

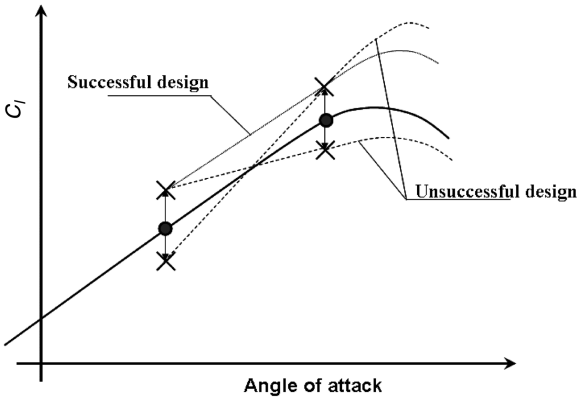

Fig. 2 High-lift system effect on airfoil lift and ideal design.

procedure to reduce the computational cost. There are several efforts about the high-fidelity optimization with considering design efficiency [6,7]. In [6], Navier–Stokes design of a high-lift system based on finite difference sensitivity evaluation was performed with a few design iterations. In [7], Kriging surrogate model was introduced to perform the global optimization and reduce the total computational cases.

In this study, Kriging surrogate model and multi-objective genetic algorithm (MOGA) is applied to multi-objective design problem. The three-element airfoil as shown in Fig. 1 is used as a baseline setting. The geometry is the wing cross section of the scaled aircraft model for the wind tunnel test of high-lift system in JAXA [8–10].

Generally, a slat increases the stall angle and a flap produces an upward shift in a lift curve as shown in Fig. 2 [1], thus multi-angle of attack should be considered. In this study, the multi-objective design of the three-element high-lift system is defined, where objective functions are to maximize C_l at the angle of attack of 8 and 20 deg. The angle of attack of 8 deg corresponds to landing condition, and the angle of attack of 20 deg corresponds to near-stall angle. The design variables are elements' settings.

The Kriging surrogate model allows efficient searching process, resulting in drastic reduction in computational time. In this study, two Kriging surrogate models corresponding to each objective functions are constructed. Expected improvement (EI) value [7,11] calculated on the Kriging surrogate model is used as a criterion to select additional sample points after Kriging surrogate models are constructed using initial samples. They make it possible not only to improve the accuracy of the Kriging surrogate model but also to explore the global optimum efficiently. EI values are maximized using divided range MOGA (DRMOGA) [12,13], which is one of the modified versions of MOGA.

Formulation

Flow Solver

Aerodynamic performances of sample designs for Kriging surrogate models are evaluated using a structured multiblock flow solver, Unified Platform for Aerospace Computational Simulation (UPACS) [14]. UPACS is developed at Japan Aerospace Exploration Agency (JAXA) as a common-base code for aerodynamic researchers.

In this study, Reynolds-averaged Navier–Stokes simulations (RANS) are applied using Spalart–Allmaras turbulence model [15]. Flux was evaluated by Roe's flux difference splitting with MUSCL for third-order spatial accuracy. The computational grid as shown in Fig. 3 is decomposed into 35 subdomains. The number of cells is about 10,000. To reduce mesh generation time, the deforming mesh method [16] is applied to deform the mesh around the baseline

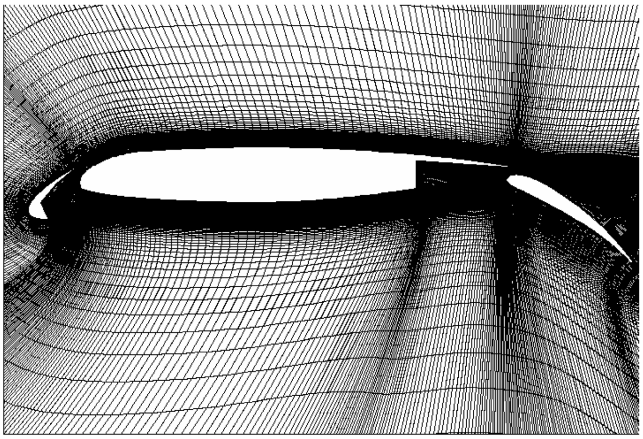

Fig. 3 Near view of computational grid for three-element airfoil.

setting. The Mach number is set to 0.2 and the Reynolds number is set to 1.24×10^7 normalized by c. The minimum spacing around the boundary layer is set to $0.01/\sqrt{Re}$ and the outer boundary is set to $100c$.

Design Variables

As shown in Fig. 4, the overlap, the gap, and the deflection angle between elements are used as the design variables. Each design variable in limited as follows:

$$-0.01c \le \text{overlap}_{\text{slat}} \le 0.01c \qquad 0.01c \le \text{gap}_{\text{slat}} \le 0.04c$$

$$20.0 \le \theta_{\text{slat}} \le 30.0 \text{ deg} \qquad -0.01c \le \text{overlap}_{\text{flap}} \le 0.01c$$

$$0.01c \le \text{gap}_{\text{flap}} \le 0.03c \qquad 30.0 \le \theta_{\text{flap}} \le 40.0 \text{ deg}$$

The design space was determined based on practical use in this case.

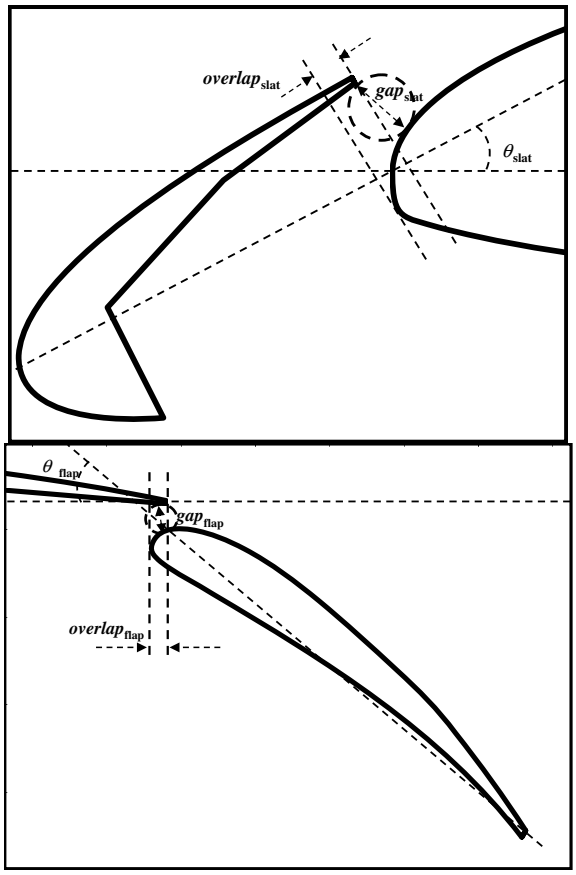

Fig. 4 Design parameters for elements' setting.

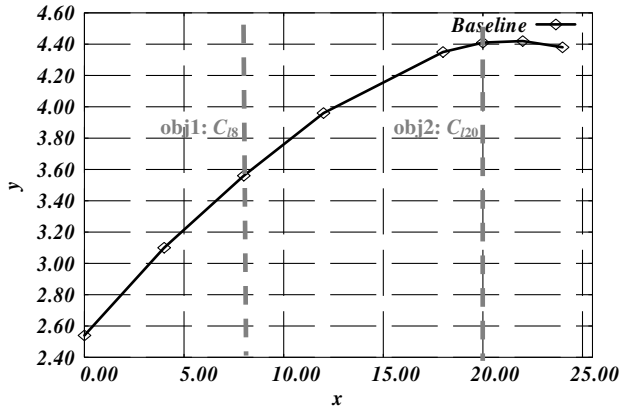

Fig. 5 Lift coefficient for baseline configuration.

Objective Functions

In this study, the design problem has two objective functions. The objectives considered here are to maximize C_l at angles of attack of 8 deg (C_{l8}) and 20 deg (C_{l20}). Angles of attack of 8 and 20 deg correspond to the angle of attack at landing condition and the stall angle decided from C_l–α of the baseline setting as discussed in the following paragraph, respectively.

The baseline setting was calculated for several angles of attack. The baseline settings (Fig. 1) are as follows:

$$\text{overlap}_{\text{slat}} = 0.005c \qquad \text{gap}_{\text{slat}} = 0.01687c \qquad \theta_{\text{slat}} = 25 \text{ deg}$$

$$\text{overlap}_{\text{flap}} = 0.01c \qquad \text{gap}_{\text{flap}} = 0.0166c \qquad \theta_{\text{flap}} = 35 \text{ deg}$$

Figure 5 shows lift curve for baseline configuration obtained by RANS. From this result, this airfoil stalled at angle of attack of 20–22 deg. From this result, the angle of attack of 20 deg was decided as the near-stall design condition.

Multi-Objective Design Exploration Based on Kriging Surrogate Model

The procedure of the present design (Fig. 6) is as follows: First, the Kriging surrogate model is constructed from N samples using Latin hypercube sampling [17], which is one of the space-filling methods. Samples are evaluated using RANS. Then, m EI maximum points are added as sample points, and the model accuracy is improved by constructing Kriging surrogate models using $N + m$ samples. This process is iterated until improvement of objective functions becomes little. Finally, data mining techniques can be applied to obtain the information of the design problem. The detail of each procedure is described in the following sections.

Kriging Surrogate Model

The Kriging surrogate model [7] expresses the value $y(x^i)$ at the unknown design point x^i as

$$y(x^i) = \mu\varepsilon(x^i) \qquad (i = 1, 2, \ldots, n_{\text{des}}) \tag{1}$$

where n_{des} is the number of design variables. The correlation between $\varepsilon(x^i)$ and $\varepsilon(x^j)$ is strongly related to the distance between the two corresponding points, x^i and x^j. In the model, the local deviation at an unknown point $\boldsymbol{x}$ is expressed using stochastic processes. Some design points are calculated as sample points and interpolated with Gaussian random function as the correlation function to estimate the trend of the stochastic process.

Improvement of the Kriging Surrogate Model and Selection of Additional Samples

Once the Kriging surrogate models are constructed, the optimum point can be explored using an arbitrary optimizer on the model. However, it is possible to miss the global optimum, because the surrogate model includes uncertainty at the predicted point. EI values [7,11] are used as the criteria in this study.

EI for present maximization problem can be calculated as follows:

$$E[I(\mathbf{x})] = (\hat{y} - f_{\max})\Phi\left(\frac{\hat{y} - f_{\max}}{s}\right) + s\phi\left(\frac{\hat{y} - f_{\max}}{s}\right) \tag{2}$$

where $\hat{y}$ is the value predicted by Eq. (1) at an unknown point $\boldsymbol{x}$. EI considers the predicted function value and its uncertainty simultaneously. Thus, the solution that has a large function value and a large uncertainty may be a promising solution. Therefore, by selecting the point where EI takes the maximum value as the additional sample point, robust exploration of the global optimum and improvement of the model can be achieved simultaneously because this point has a somewhat large probability to become the global optimum. To apply multi-objective problem, this study considers two EI values based on two Kriging surrogate models: EI_{Cl8} and EI_{Cl20}. Equation (2) can be written for the present design problem as follows:

$$\begin{aligned}
&\text{maximize}: \text{EI}_{Cl8} = (\hat{y} - C_{l8_{\max}})\Phi\left(\frac{\hat{y} - C_{l8_{\max}}}{s}\right) + s\phi\left(\frac{\hat{y} - C_{l8_{\max}}}{s}\right) \\
&\text{maximize}: \text{EI}_{Cl20} = (\hat{y} - C_{l20_{\max}})\Phi\left(\frac{\hat{y} - C_{l20_{\max}}}{s}\right) \\
&\quad + s\phi\left(\frac{\hat{y} - C_{l20_{\max}}}{s}\right)
\end{aligned} \tag{3}$$

Maximizing these objective functions, nondominated solutions between EI_{Cl8} and EI_{Cl20} can be obtained. Among these nondominated solutions, three points are selected as additional sample points (Fig. 7): 1) the point whose EI values of C_{l8} is maximum, 2) the point whose EI values of C_{l20} is maximum, and 3) the midpoint in the nondominated solutions. Therefore, the value of m becomes 3 in this study.

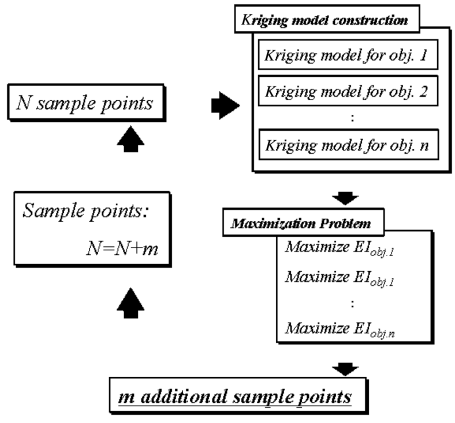

Fig. 6 Procedure of multi-objective global exploration.

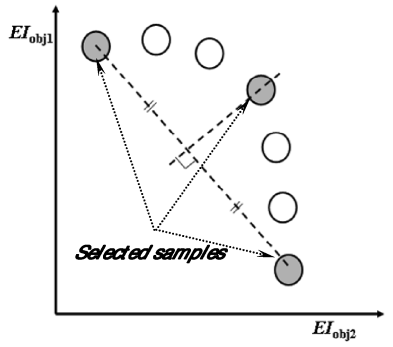

Fig. 7 Selection of additional samples based on EI maximization.

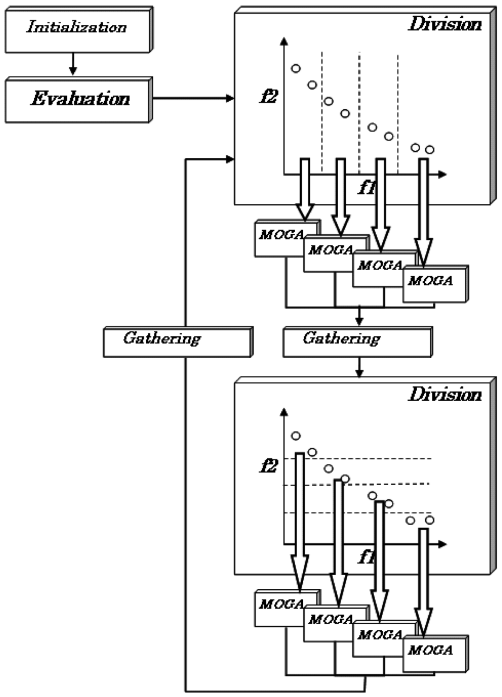

Fig. 8 Procedure of divided range MOGA.

DRMOGA

DRMOGA is characterized by the parallelization model where the individuals are divided into subpopulations. There is evidence indicating the good performance of DRMOGA at maintaining diversity and converging closer to the true Pareto front than previous MOGA [12,13]. The subdivision of the population based on alternative objective functions prevents the premature convergence to a nondominated solution segment and introduces migration of individuals to neighboring nondominated solution segments. A comparison of results produced by DRMOGA and previous MOGA was also performed to verify the performance of the optimization of DRMOGA for the practical application.

The DRMOGA procedure shown in Fig. 8 can be explained as follows [12,13]. First, initial individuals are produced randomly and evaluated. Second, the division of individuals is performed by using the rank of individuals based on values of a certain objective function f_i. Assuming n subpopulations for N individuals, N/n individuals will be allocated to each subpopulation. Then in each subpopulation, the existing MOGA [12] is performed. After MOGA is performed for k generations, all of the individuals are gathered and they are divided into subpopulations again according to the ranking based on another objective function f_j. This ranking function will be chosen in turn. For present DRMOGA, k was set to 4 and the number of subpopulations n was set to 4.

Data Mining Technique: ANOVA

One of the advantages of using a surrogate model is that it shows the relationship between the objective and design variables. This relationship is very helpful to identify how much influence each design variable has on the objective. To evaluate the effect of each design variable, the total variance of the model is decomposed into that of each design variables and interactions.

An analysis of variance (ANOVA) [18], which is one of the data mining techniques, is carried out to differentiate the contributions to the variance of the response from Kriging surrogate model. The decomposition is accomplished by integrating variables out of the model $\hat{y}$. The main effect of design variable x_i is as follows:

$$\mu_i(x_i) \equiv \int \cdots \int \hat{y}(x_1, \ldots, x_n)\, \mathrm{d}x_1, \ldots, \mathrm{d}x_{i-1}, \mathrm{d}x_{i+1}, \ldots, \mathrm{d}x_n - \mu \tag{4}$$

Two-way interaction effect x_i and x_j is written as

$$\mu_{i,j}(x_{i,j}) \equiv \int \cdots \int \hat{y}(x_1, \ldots, x_n)\, \mathrm{d}x_1, \ldots, \mathrm{d}x_{i-1}, \mathrm{d}x_{i+1} \ldots, \mathrm{d}x_{j-1}, \mathrm{d}x_{j+1}, \ldots, \mathrm{d}x_n - \mu_i(x_i) - \mu_j(x_j) - \mu \tag{5}$$

where total mean μ is as follows:

$$\mu \equiv \int \ldots \int \hat{y}(x_1, \ldots, x_n)\, \mathrm{d}x_1, \ldots, \mathrm{d}x_n \tag{6}$$

The variance due to the design variable x_i is

$$\varepsilon_{\text{main}} \equiv \int [\mu_i(x_i)]^2\, \mathrm{d}x_i \tag{7}$$

The proportion of the variance due to design variable x_i to total variance of the model can be expressed as

$$p_{\text{main}} \equiv \frac{\varepsilon_{\text{main}}}{\int \ldots \int [\hat{y}(x_1, \ldots, x_n) - \mu]^2\, \mathrm{d}x_1 \ldots, \mathrm{d}x_n} \tag{8}$$

The variance due to the design variables x_i and x_j is

$$\varepsilon_{\text{inter}} \equiv \iint [\mu_{i,j}(x_{i,j})]^2\, \mathrm{d}x_i\, \mathrm{d}x_j \tag{9}$$

The two-way interaction due to design variables x_i and x_j can be expressed as

$$p_{\text{inter}} \equiv \frac{\varepsilon_{\text{inter}}}{\int \ldots \int [\hat{y}(x_1, \ldots, x_n) - \mu]^2\, \mathrm{d}x_1 \ldots, \mathrm{d}x_n} \tag{10}$$

The denominators of Eqs. (8) and (9) mean variance of the model.

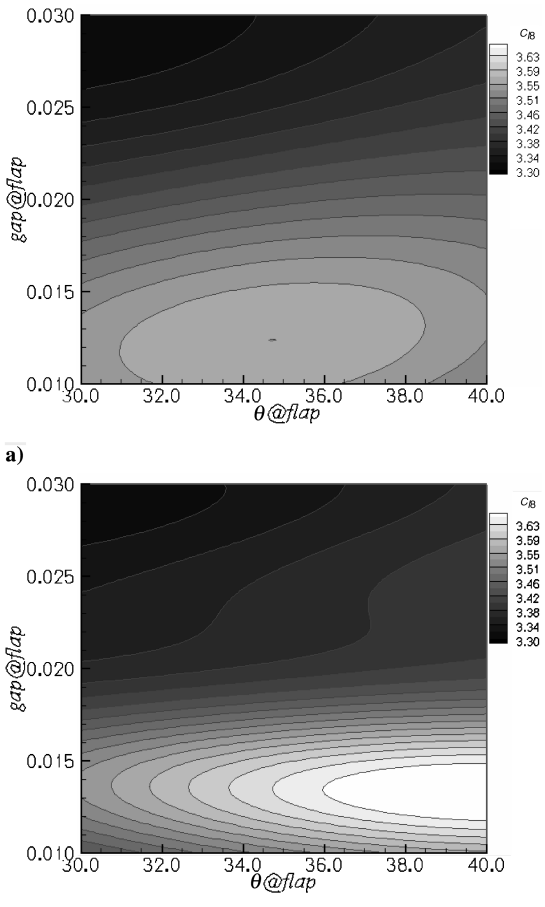

Fig. 9 C_{l8} plots predicted by the Kriging surrogate model about θ_{flap}–gap_{flap}: a) from initial samples, b) from final 90 samples.

The values obtained by Eqs. (8) and (9) indicate the sensitivity of the objective function to the variation of the design variable.

Results

Kriging Surrogate Model

First, to construct the initial Kriging surrogate model, 30 sample designs were evaluated by RANS. Then, to explore better solutions based on EI maximization, the samples were added 20 times. As a result, 60 samples were added and final Kriging surrogate model was constructed using 90 samples.

Figures 9a and 9b show C_{l8} plots against θ_{flap}–gap_{flap} predicted by Kriging surrogate model obtained from initial 30 sample designs and final 90 samples, respectively. According to Fig. 9, a smaller gap between a flap and a main wing produces higher C_{l8}. Besides, Fig. 9b shows that larger deflection of flap (around 39 deg) produces higher C_{l8} than Fig. 9a. Moreover, the Kriging surrogate model improved and the maximum of C_{l8} increased; therefore, the design range that shows better aerodynamic performance emerged. This result shows that the present method can find the optimum by the additional sampling.

Figures 10a and 10b show C_{l20} plots against θ_{slat}–gap_{slat} predicted by Kriging surrogate model obtained from initial 30 sample designs and additional samplings, respectively. According to Fig. 10, the design point achieving maximum C_{l20} moved and the accuracy of the Kriging surrogate model around the maximum point of C_{l20} was improved.

Comparison of Solutions Chosen from Sampling Result

Figure 11 shows the solutions obtained based on the present method. From this figure, the uniform initial distribution of the solutions obtained from the initial sampling can be observed. On the other hand, the solutions obtained from 15th–20th additional samplings achieve the better performance than that of the initial samplings. The nondominated front gradually advances to the optimum direction as the improving process is proceeded. These results indicated that the present method selects the additional samples properly.

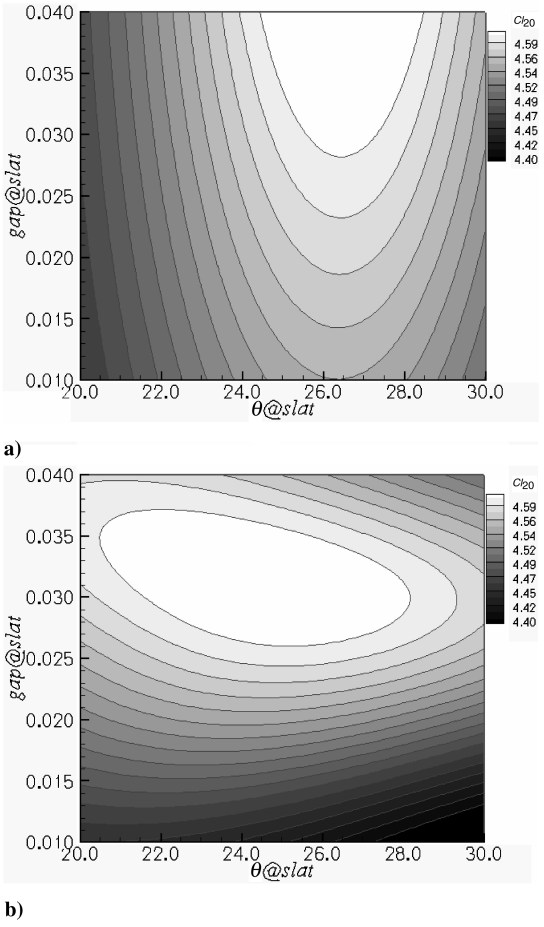

Fig. 10 C_{l20} plots predicted by the Kriging surrogate model about θ_{slat}–gap_{slat}: a) from initial samples, b) from final 90 samples.

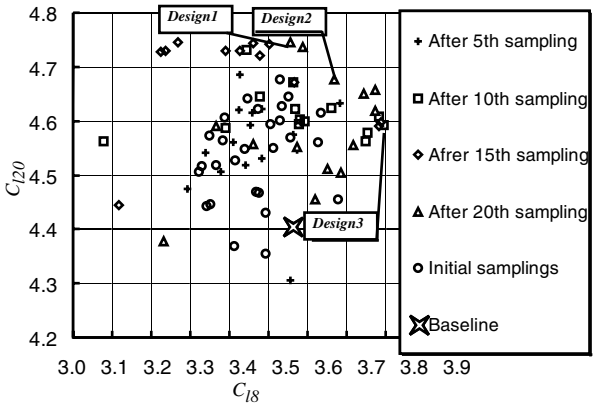

Fig. 11 Sample points obtained based on EI maximization.

The elements' settings obtained from additional samplings (designs 1, 2, and 3 shown in Fig. 11) are compared. Figure 12 illustrates the comparison of their settings with the baseline setting. Every selected design dominates the baseline setting in the solution space. Thus, these settings have similar characteristics; the gap of slat and the deflection angle of flap is larger.

C_p distributions of the baseline and the selected designs are compared as shown in Figs. 13–15. According to Fig. 13b, the suction peak at the leading edges of the mother element and the flap of the design 1 are higher than that of the baseline; thus, design 1 achieves highest C_{l20}. According to Figs. 13a and 14a, the C_p value on the upper surface of the mother element of the design 2 is lower

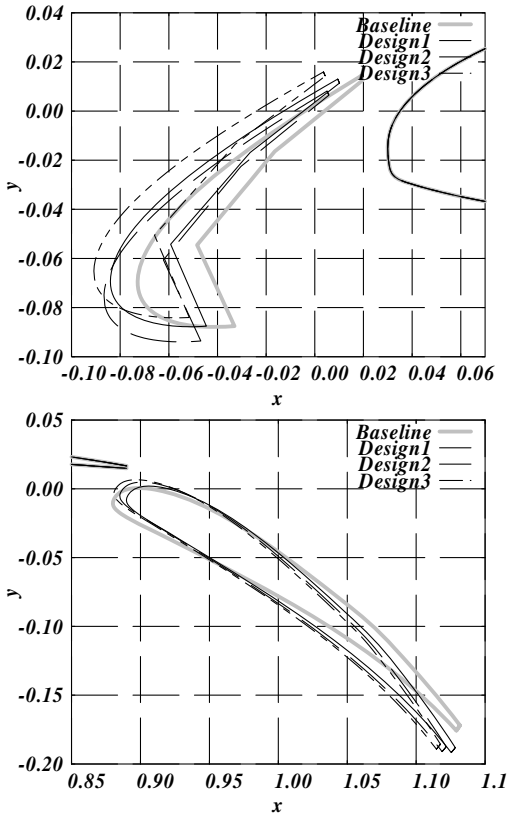

Fig. 12 Comparison of elements' settings among baseline configuration and designed configurations.

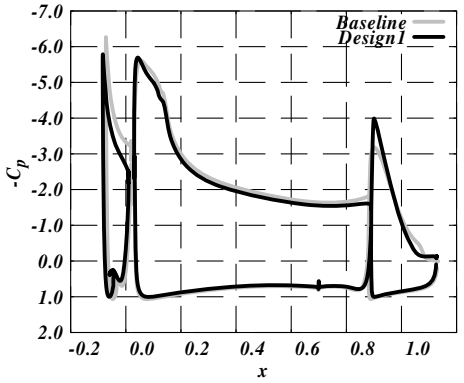

a)

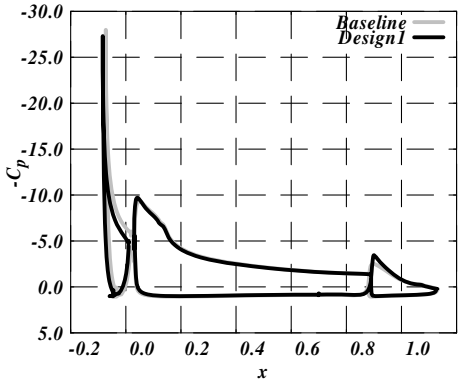

b)

Fig. 13 Comparison of C_p distributions between baseline configuration and design 1: a) $\alpha = 8$ deg, b) $\alpha = 20$ deg.

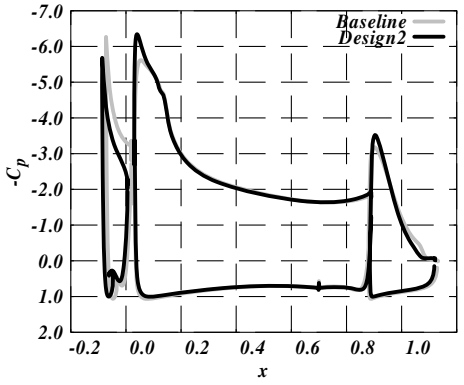

a)

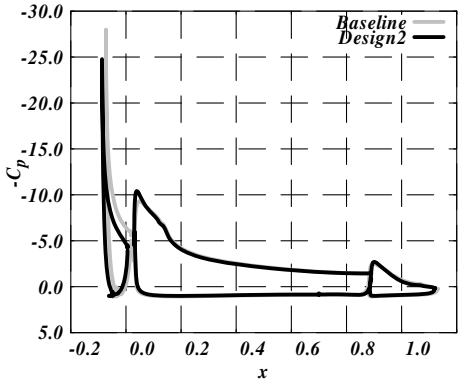

b)

Fig. 14 Comparison of C_p distributions between baseline configuration and design 2: a) $\alpha = 8$ deg, b) $\alpha = 20$ deg.

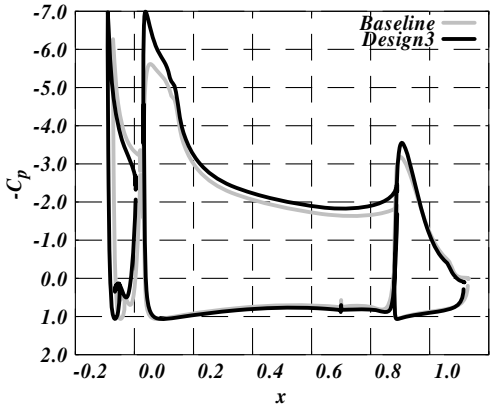

a)

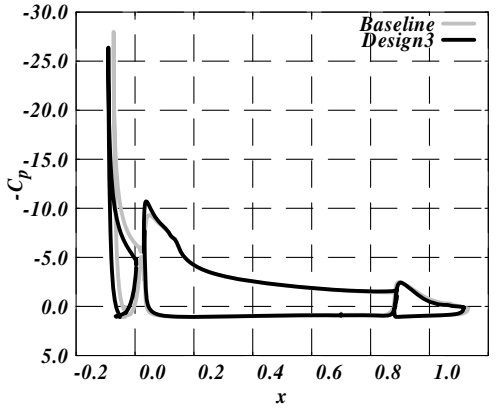

b)

Fig. 15 Comparison of C_p distributions between baseline configuration and design 3: a) $\alpha = 8$ deg, b) $\alpha = 20$ deg.

than that of the design 1. As a result, C_{l8} of the design 2 is higher than that of design 1. Figure 15a shows that C_p value on the upper surface of the mother element of the design 3 is lower than that of the baseline. Consequently, design 3 achieves the highest C_{l8}.

Figure 16 shows the comparison of C_l–α curve among designs 1–3 and the baseline. The C_l–α curve of design 2 and 3 is above the baseline. Besides, the angle of attack that shows the maximum C_l becomes larger than that of the baseline. This result suggests that the present design can produce the ideal elements' setting explained in Fig. 2. On the other hand, C_{l8} of the design 1 does not become so higher than that of the baseline setting, whereas C_{l20} becomes higher. As a result, the gradient of the C_l curve becomes large. This result suggests that to improve C_l curve, multi-angle design is required.

Result of ANOVA

Total variances of Kriging surrogate models were decomposed into the variance due to each design variable. The proportion to the total variable of design variables and their interactions are shown in Fig. 17. According to Fig. 17a, the flap setting gives over 70% effect on the C_{l8}. Moreover, according to this figure, the two-way interaction between $\text{overlap}_{\text{flap}}$ and gap_{flap} has a large effect on C_{l8}. This result suggests that $\text{overlap}_{\text{flap}}$ and gap_{flap} should be designed considering their interaction carefully. Besides, θ_{flap} has a relative small effect because the maximum point of C_{l8} exists around the upper bound of θ_{flap} (see Fig. 9b). According to Fig. 17b, the slat and the flap setting both give effect on the C_{l20}. This result suggests that the proper setting of elements for C_{l20} is more difficult than that for C_{l8}. According to this figure, the gap of flap is also an important design variable for each objective. Generally, a slat is set to increase stall angle; however, this result suggests that the flap setting is also important for the aerodynamic performance near-stall condition. Not only slat but also flap should be designed carefully for near-stall condition.

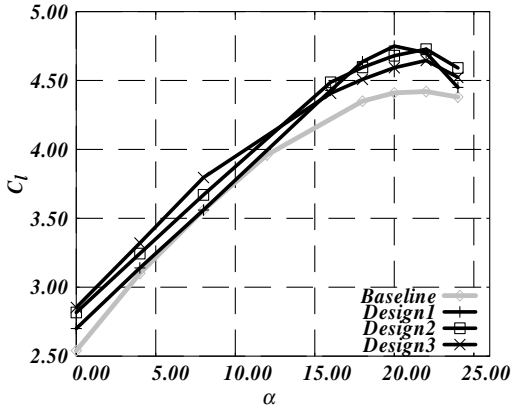

Fig. 16 Comparison of C_l–α among selected solutions.

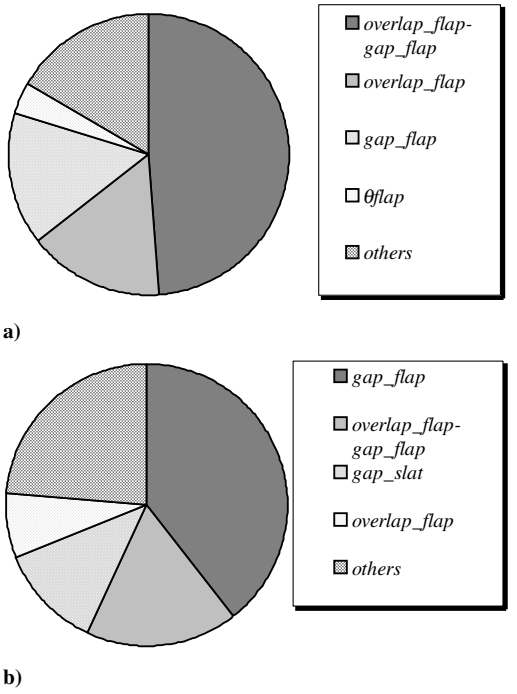

Fig. 17 Total proportion to the total variance of models: a) C_{l8}, b) C_{l20}.

Conclusions

Multi-objective design for the elements' settings of the high-lift airfoil consisting of a slat, a main wing, and a flap was performed based on MOGA exploration on the Kriging surrogate models. Kriging surrogate model was used to reduce computational cost. There were two objective functions: maximizing lift coefficient at a landing condition (C_{l8}) and maximizing lift coefficient at near-stall condition (C_{l20}). Flowfields were simulated by solving the Navier–Stokes equations with Spalart–Allmaras turbulent model using the multiblock structured grid method. The computational grids were deformed automatically for each design.

In this study, the objective functions, C_{l8} and C_{l20}, were transformed to the corresponding EI values on the Kriging surrogate model, and global optimization was performed based on maximizing their values. Using Kriging surrogate model, the computational cost can be reduced and EI value can be permitted to carry out high efficient design on the Kriging surrogate model. To explore the maximum EI values, DRMOGA, a modified version of MOGA, was used. The resulting designs were also used as the additional samples to update the Kriging surrogate models.

Through the present method, the solutions based on the EI maximization advanced to the optimum direction in the solution space. As the result, element settings that give higher performance than that of baseline were successfully obtained. This result suggests that the present method using the Kriging-based MOGA can be applied to the multi-objective problem while reducing computational time drastically.

To obtain the information about design space, ANOVA, which is one of the data mining techniques, is applied to the sampling result. This result shows the useful information for the design. C_{l8} is mainly improved by flap setting. On the other hand, to improve C_{l20}, not only slat setting but also flap setting should be considered. Generally, it is said that slat is effective to improve the C_l at high angle of attack. However, the slat and the flap settings have interaction at high angle of attack.

References

[1] van Dam, C. P., "The Aerodynamic Design of Multi-Element High-Lift Systems for Transport Airplanes," *Progress in Aerospace Sciences*, Vol. 38, No. 2, Feb. 2002, pp. 101–144.

[2] Smith, A. M. O., "High-Lift Aerodynamics," *Journal of Aircraft*, Vol. 12, No. 6, 1975, pp. 501–530.

[3] Murayama, M., Lei, Z., Mukai, J., and Yamamoto, K., "CFD Validation for High Lift Devices: Three-Element Airfoil," *Transactions of the Japan Society for Aeronautical and Space Sciences*, Vol. 49, No. 163, May 2006, pp. 40–48.

[4] Mani, M., and Bushm R. H., "Overlapping Grid Method for High-Lift and Store Carriage Applications," AIAA Paper 93-3428, 1993.

[5] Mathias, D. L., and Cummings, R. M., "Navier-Stokes Analysis of the Flow About a Flap Edge," *Journal of Aircraft*, Vol. 35, No. 6, 1998, pp. 833–838.

[6] Eyi, S., Lee, K. D., Rogers, S. E., and Kwak, D., "High-Lift Design Optimization Using Navier-Stokes Equations," *Journal of Aircraft*, Vol. 33, No. 3, 1996, pp. 499–504.

[7] Jeong, S., Murayama, M., and Yamamoto, K., "Efficient Optimization Design Method Using Kriging Model," *Journal of Aircraft*, Vol. 42, No. 2, 2005, pp. 413–420.

[8] Imamura, T., Enomoto, S., and Yamamoto, K., "3D Unsteady Flow Computations in a Slat Cove Using Large Eddy Simulation," AIAA Paper 2006-2668, 2006.

[9] Yokokawa, Y., Murayama, M., Ito, T., and Yamamoto, K., "Experiment and CFD of a High-Lift Configuration Civil Aircraft Model," AIAA Paper 2006-3452, 2006.

[10] Ura, H., Yokokawa, Y., and Ito, T., "Phased Array Measurement of High Lift Device in Low Speed Wind Tunnel," AIAA Paper 2006-2565, 2006.

[11] Donald, R., J., Matthias, S., and William, J. W., "Efficient Global Optimization of Expensive Black-Box Function," *Journal of Global Optimization*, Vol. 13, No. 4, Dec. 1998, pp. 455–492.

[12] Hiroyasu, T., Miki, M., and Watanabe, S., "The New Model of Parallel Genetic Algorithm in Multi-Objective Optimization Problems (Divided Range Multi-Objective Genetic Algorithm)," *IEEE Proceedings of the Congress on Evolutionary Computation 2000*, Vol. 1, IEEE Publications, Piscataway, NJ, 2000, pp. 333–340.

[13] Kanazaki, M., Obayashi, S., and Nakahashi, K., "Exhaust Manifold Design with Tapered Pipes Using Divided Range MOGA," *Engineering Optimization*, Vol. 36, No. 2, 2004, pp. 149–164.

[14] Takaki, R., Yamamoto, K., Yamane, T., Enomoto, S. and Mukai, J., "The Development of the UPACS CFD Environment," *High Performance Computing, Proceedings of ISHPC 2003*, Springer, New York, 2003, pp. 307–319.

[15] Spalart, P. R., and Allmaras, S. R., "A One-Equation Turbulent Model for Aerodynamic Flow," AIAA Paper 92-0439, 1992.

[16] Crumpton, P. I., and Giles, M. B., "Implicit Time Accurate Solutions on Unstructured Dynamic Grids," AIAA Paper 95-1671-CP, 1995, pp. 284–294.

[17] Mckay, M. D., Beckman, R. J., and Conover, W. J., "A Comparison of Three Methods for Selecting Values of Input Variables in the Analysis of Output from a Computer Code," *Technometrics*, Vol. 21, No. 2, 1979, pp. 239–245.

[18] Sack, J., Welch, W. J., Mitchell, T. J., and Wynn, H. P., "Design and Analysis of Computer Experiments (with Discussion)," *Statistical Science*, Vol. 4, No. 4, Nov. 1989, pp. 409–435.